ASTRONOMY & ASTROPHYSICS SUPPLEMENT SERIES

DECEMBER II **1995**, PAGE 489

Astron. Astrophys. Suppl. Ser. **114,** 489-497 (1995)

$UBVRI$-CCD photometry of Cepheus OB3 association*,**

C. Jordi[1], D. Galadí-Enríquez[1], E. Trullols[1,2] and F. Lahulla[3]

[1] Departament d'Astronomia i Meteorologia, Universitat de Barcelona, Avda. Diagonal 647, E-08028 Barcelona, Spain
[2] Departament de Matemàtica Aplicada i Telemàtica, Universitat Politècnica de Catalunya, Avda. Victor Balaguer s/n, E-08800 Vilanova i la Geltrú, Spain
[3] Observatorio Astronómico Nacional, Alfonso XII 3, E-28014 Madrid, Spain

Received March 9; accepted June 14, 1995

Abstract. — Johnson CCD photometry was performed in the two subgroups of the association Cepheus OB3, for selected fields each containing at least one star with previous UBV photoelectric photometry. Photometry for about 1000 stars down to visual magnitude 21 is provided, although the completeness tests show that the sample is complete down to V=19 mag. Individual errors were assigned to the magnitude and colours for each star. Colour-colour and colour-magnitude diagrams are shown. Astrometric positions of the stars are also given. Description of the reduction procedure is fully detailed.

Key words: open clusters and associations: individual: Cepheus OB3 — techniques: photometric — HR diagram — astrometry

1. Introduction

The association Cepheus OB3, in the sky region between $22^{\rm h}46^{\rm m} < \alpha_{2000} < 23^{\rm h}10^{\rm m}$ and $+61^\circ < \delta_{2000} < +64^\circ$ ($l \approx 110^\circ$, $b \approx 3^\circ$), is a typical stellar association placed at about 725 pc from the Sun. Compared to other nearby stellar associations (Blaauw 1964, 1991; Garmany 1992) it is a rather modest group. However, Cepheus OB3 is one of the clearest examples of sequential star formation, with a structure in two subgroups aligned almost parallel to the galactic plane. The two subgroups show evidence of being in different evolutionary stages, both by their spatial concentration and by their stellar content. The association interacts with the interstellar medium, mainly the youngest subgroup. There are strong signs of current stellar formation inside Cepheus-A, the densest concentration of the Cepheus molecular cloud (Sargent 1979; Huges 1988), south-west from the association.

The studies of Cepheus OB3 performed to date have been based on a list of members proposed by Blaauw et al. (1959; hereafter referred to as BHJ) including stars down to photographic magnitude around 12.5 (spectral type B5). On the one hand, the spatial boundaries of the association are not well defined. The outer regions of OB associations are sparsely populated, merging and mixing with the field population. The largest overall projected diameter for the young and old subgroups of Cepheus OB3 have been quoted by Blaauw to be 10 and 17 pc, respectively, but the individual distances computed for the members range from 500 to 1000 pc (Crawford & Barnes 1970). Jordi et al. (1992) have found stars compatible with being members of Cepheus OB3 that would increase the angular diameters of the subgroups. On the other hand, little is known about the membership of faint stars in this and other associations. As Blaauw (1964) pointed out, the number of faint members of the associations appears not to increase rapidly with decreasing luminosity. So, the stellar associations do not stand out with respect to the galactic background. The lack of faint members could be due to incompleteness of the observations: simply, they have not been studied because of the great observational effort required.

However, knowledge of the stellar content of the associations could provide important information about the process of star formation, the initial mass function and the premain sequence members (Garmany 1994). Late B, A and F-type stars have been found in Sco OB2 (Garrison 1967; de Geus et al. 1989) and Ori OB1 (Brown et al. 1994). Our purpose is to perform a similar search in Cepheus OB3. Since Sco OB2 and Ori OB1 are near the Sun, the magnitudes under study are still within the range of photoelectric photometry. However, since Cepheus OB3 is further, the use of CCD is a more obvious choice.

In this paper, we present $UBVRI$ CCD-photometry for about 1000 stars in selected fields of Cepheus OB3. We leave the analysis of this photometry and the membership determination for the observed stars for a second paper.

*Based on observations made at Centro Astronómico Hispano-Alemán, Almería, Spain

**Table 5 is only available in electronic form from CDS via anonymous ftp 130.79.128.5, and by e-mail request to C. Jordi at carme@facjn0.am.ub.es

Table 1. Quantum efficiency γ of GEC#10 as a function of wavelength λ

λ (nm):	350	400	500	600	700	800	900
γ (%):	17	18	20	42	55	43	15

Table 2. Chip specifications

Type:	GEC#10 coated
Dimensions (pixels):	385 × 576
Pixel size:	22 μm = 0.46″
Field of view:	3.0′ × 4.4′
Sensitivity:	5.7 e^-/ADU
Temperature:	154 K
Read-out-noise:	2.3 ADU
Dynamical range:	65535 ADU
Linear up to:	40000 ADU
Typical bias level:	260 ADU
Overscan region:	yes (right-left)

2. Observations

The observations were carried out during seven nights in November 1991 and one night in October 1993, six of which were of good photometric quality. The instrument was the 1.23 m telescope of Centro Astronómico Hispano-Alemán (CAHA) at Calar Alto (Almería, Spain), using a coated chip GEC#10 in the CCD direct imaging camera. Quantum efficiency and chip specifications are given in Tables 1 and 2, respectively. Filters used are compared with standard *UBVRI* Johnson-Cousins filters (Bessel 1993) in Table 3.

Table 3. Used and standard filters of *UBVRI* Johnson-Cousins system

Filter:	*U*	*B*	*V*	*R*	*I*
			Used		
Central λ (nm):	366.0	448.5	535.9	641.3	900.0[a]
FWHM (nm):	52.0	75.9	90.1	159.0	100.0[a]
Thickness (mm):	2.9	8.0	4.0	4.0	3.0
			Standard		
Central λ (nm):	367	436	545	638	797
FWHM (nm):	66	94	88	138	149

[a]Uncertain due to the lack of calibration.

Frames were obtained for 11 fields in the region of the youngest subgroup and for 7 in the oldest region, non-overlaping and randomly selected, each surrounding one of the BHJ stars. Exposure times were 2000, 1000, 500, 100 and 200 s for filters U, B, V, R and I, respectively. These times were the result of a compromise between the time available and a good signal-to-noise ratio at $V = 16$ mag. Additional shorter exposures were taken when the brightest star in the field became saturated.

About 20 different Landolt (1983, 1992) standard stars per night, covering a wide range of spectral types, were observed in order to transform the instrumental system to the Johnson-Cousins standard system. Two of these standard stars were observed several times during the night, to determine atmospheric extinction. The standard stars were chosen, whenever possible, aiming to record more than one of them in the same field, to save observation time and to reduce the amount of stored data.

3. Reduction

We wish the output of the CCD camera were a two-dimensional array $Z(x,y)$ (being (x,y) the coordinates of each pixel) proportional to the incident flux of photons $I(x,y)$ and to the nominal exposure time t_n. However, the raw frame obtained reading out the chip is a two-dimensional function $\tilde{Z}(x,y)$ that can be expressed as follows:

$$\tilde{Z}(x,y) = B + D_{t_n}(x,y) + G(x,y)I(x,y)T(x,y) + S(x,y) \quad (1)$$

where

- B is the bias;
- $D_{t_n}(x,y)$ is the dark current term;
- $G(x,y)$ is the normalized flat;
- $T(x,y)$ is the total exposure time, which varies from pixel to pixel and, in general, is different from t_n due to shutter-timing effects, and
- $S(x,y)$ are the non-linear additive contributions such as read-out-noise, cosmic rays, satellite trails, chip defects, saturation, preflash, etc.

By evaluating the different contributions on the above expression one can deduce the clean frame $Z(x,y) \propto t_n I(x,y)$. The cleaning procedure is described in the following subsection, and it is schematized in Fig. 1.

3.1. *Preliminary treatment of the frames*

Bias level was evaluated individually for each frame by averaging the counts of the most stable pixels in the overscan areas.

Dark exposures were obtained throughout the observation period to evaluate the dark field pattern and its possible dependence on the exposure time, as $D_{t_n}(x,y) = D(x,y) + k(x,y)t_n$. The bias level was subtracted from each individual dark field, and a cosmic ray cleaning procedure was applied. Dark frames of same exposure time were averaged afterwards to decrease the read-out-noise and to reveal the structure of the dark current. All dark frames show a very low count level (average of 0.57 ADU), their two-dimensional structure is not very important (σ =0.73 ADU) and their dependence on time is negligible for our

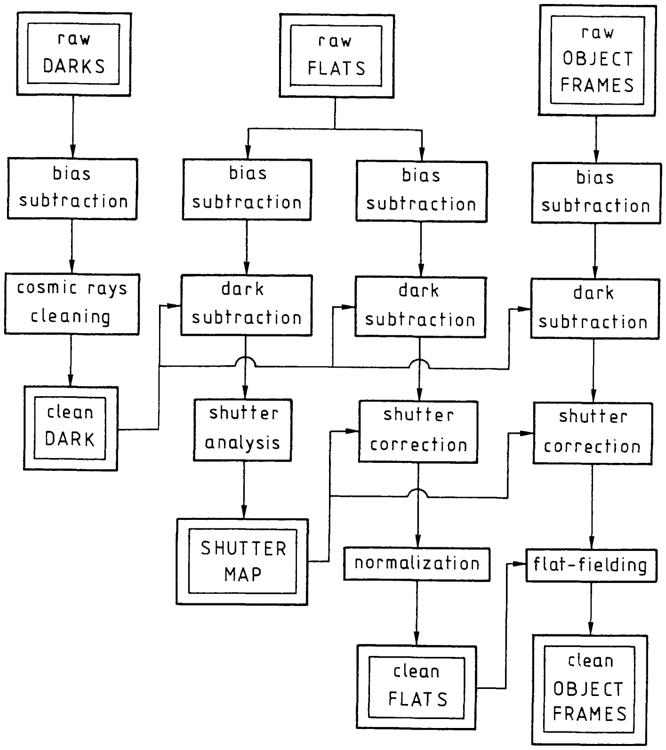

Fig. 1. Treatment of the raw frames to obtain the clean frames

exposure times. So, we have adopted $D_{t_n}(x,y) = D(x,y)$ obtained by averaging all dark frames of each observational run.

Due to the fact that CCD shutters take a finite time to open and close, the total time $T(x,y)$ during which a pixel (x,y) has been exposed is different from the nominal time t_n, the difference being a two-dimensional function $\delta(x,y) = T(x,y) - t_n$ that depends on the shape of the shutter and the way it opens and closes. The shutter of the GEC#10 has been analyzed by Galadí-Enríquez et al. (1994) generalizing Stetson (1989). The shutter map $\delta(x,y)$ computed for the night of October 1993 is shown in Fig. 2. It is worth noticing the difference of 0.1 s between the most and least exposed pixels and the 0.3 s over-exposure common to all of them. The shutter-timing affects the images not only directly, but also indirectly via the flat-fielding process, since the shutter map is mixed up with the true flat field pattern, mainly if flat fields are taken with short exposure times. Both direct and indirect effects can be easily removed by applying a factor $t_n/[t_n + \delta(x,y)]$ both to flat-field and to object frames.

Dome flat frames were acquired to normalize the response of each pixel. Bias and dark current were subtracted from the frames. Shutter-timing effect was also removed. The clean flat frames show the same two-dimensional structure irrespective of the level of the illumination and are similar for all the filters. The normalized flat frames adopted are the average of about 15 different flat frames for each filter and each observational run.

The frames were processed using the ESO's image processing software MIDAS running in an IBM AIX6000 Mod.540.

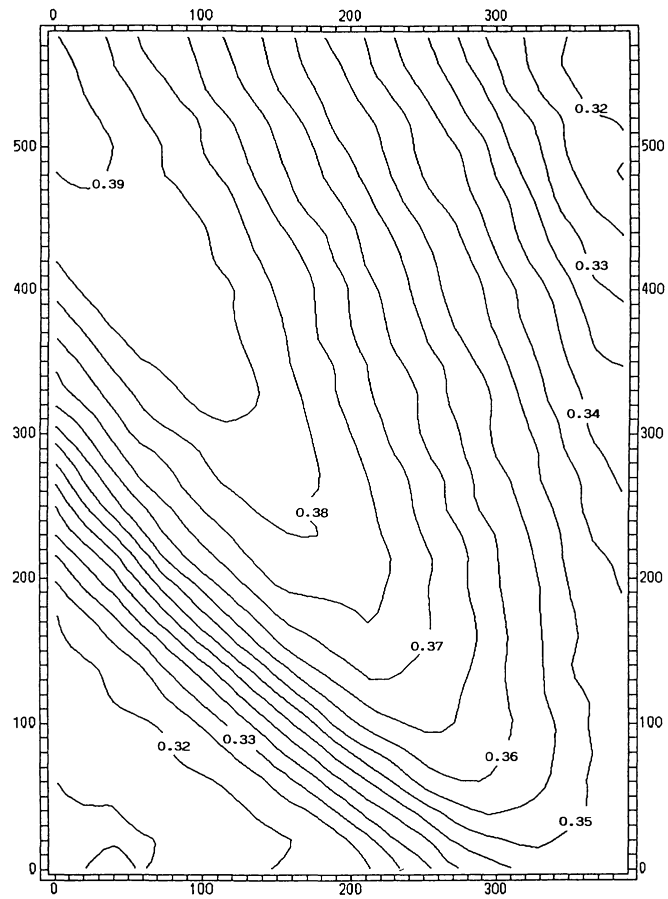

Fig. 2. Shutter map, $\delta(x,y) = T(x,y) - t_n$, of the GEC♯10 at 1.23 m telescope in October 1993. Units are seconds

3.2. *Instrumental magnitudes*

The instrumental magnitudes from the clean images $Z(x,y)$ were obtained using the DAOPHOT and DAOGROW programs (Stetson 1987, 1990).

The FIND command of DAOPHOT was used to detect the stars present in each frame. This command needs the approximated FWHM of the star images and it runs accepting as stars the images of objects whose geometrical shape, described by two parameters (*sharp* and *round*), lies between the limits imposed by the user. The user also sets a minimum *threshold* level beneath which every detection is considered as noise.

Two processes are normally used to obtain photometry from a two-dimensional digitized image: the aperture synthesis and the profile-fitting methods (see Da Costa 1992 for a good understandable comparison). The aperture synthesis is the digital counterpart of photoelectric photometry. It consists in integrating the recorded total intensity inside a given radius around the star centre (which acts as a synthetic diaphragm) and subtracting the sky value evaluated from pixels close to the star. On the other hand, the profile-fitting method fits a two-dimensional function (PSF) to bright and well isolated stars in the frame, and the intensity integration is performed not on the original pixels, but on the fitted function.

The profile-fitting method is less sensitive to defects in the image (cosmic rays for example) and is the only method suitable in crowded fields where the light of a star is contaminated by neighbouring stars, but it depends on the accuracy of the adopted PSF model and it has an arbitrary zero point. The actual zero point must be scaled by means of the aperture synthesis photometry. So, the accuracy of PSF photometry is limited by the accuracy of this zero point fitting.

Since our fields are not crowded, we decided to use the aperture synthesis method (using the PHOT command in DAOPHOT program). PHOT uses the star centres determined by FIND and gives the instrumental magnitudes for each of twelve circles with radii chosen by the user. The instrumental magnitudes are given as $m = 25 - 2.5\log_{10}\sum_{xy}[Z(x,y) - f_c]$, where f_c is the sky value evaluated from an annulus with radii also chosen by the user.

If seeing, guiding or focusing changed significantly between one frame and another, the amount of missing (i.e. not measured) stellar flux using a given aperture will differ from frame to frame and the zero point of the instrumental magnitudes will be unstable. Theoretically, this effect can be avoided for isolated stars by integrating the total flux using a very large aperture. However, although a very large aperture includes, in principle, all the stellar flux, its signal-to-noise ratio is lower than for a relatively small radius (Howell 1989, among others) due to the other sources of error. One should choose the aperture with maximum signal-to-noise ratio and extrapolate the stellar flux measured through it to infinite aperture applying what is known as the *aperture correction* (Da Costa 1992).

We analyzed the magnitude growth curves and determined the aperture correction with the DAOGROW program. From the instrumental magnitudes given by PHOT, DAOGROW computes a uniparametric family of growth curves for all the frames using the FWHM of the stellar images as free parameter. The analytic-synthetic procedure gives high weight to the empirical growth curves for the smallest apertures, and to a theoretical stellar profile (King 1971) for the largest apertures. This process minimizes the effect of possible defects in the image, contamination due to nearby stars and erroneous background determination.

Due to the large number of frames to treat (about 500) with different FWHM due to the variation of the seeing along the observational period, we applied an iterative procedure to obtain the instrumental magnitudes. In the first step, a preliminary value of FWHM, common to all the frames, was used to detect the stars recorded in each frame. PHOT and DAOGROW were then used to obtain the instrumental photometry and the individual FWHM of each frame. In the second step, the detection of the stars was improved by using the individual FWHM given by DAOGROW. Again, PHOT and DAOGROW were used to obtain more accurate instrumental photometry and new individual FWHM. The iteration finishes when no new stars are detected and the individual FWHM are the same as in the previous step. Two iterations were enough in our case. The frames obtained through different filters were treated separately.

3.3. *Matching frames*

The same field was measured in each of the five *UBVRI* filters, and usually with both long and short exposure times. It is necessary to cross-identify the matches of the detected stars in different frames of the same field. Again, due to the large number of frames, we decided not to do this by hand, but to use the DAOMATCH and DAOMASTER programs designed by Stetson (1993). On the basis of the conservation of angles and the ratios between sides of triangles, DAOMATCH and DAOMASTER compute transformation equations between positions and give a cross-identification list with the instrumental magnitude in each frame.

We retained only those stars appearing in at least three frames (i.e. in three filters) to ensure the computation of two independent colours. Due to the quantum efficiency of the chip (see Table 2) this limitation is equivalent to requiring the presence of the star in the V, R and I filters.

3.4. *Transformation to the standard system*

The coefficients of the transformation equations were computed by a least square method using the instrumental magnitudes of the standard stars and the standard magnitudes and colours in the Johnson-Cousins system (Landolt 1983, 1992). Those standard stars with residuals greater than 2σ were rejected. The reduction was performed for each night independently and in two steps.

In the first step, the extinction coefficients for each passband were determined. The equations used include dependence on the airmass and on a colour index. For instance, we have:

$$r - R = \text{zero point} + k_{R,VR}X_R + k'_{R,VR}X_R(V-R) \quad (2)$$

where V and R represent the standard magnitudes, r the instrumental magnitude, X_R is the airmass of the observation with the R filter, and $k_{R,VR}$, $k'_{R,VR}$ are the extinction coefficients. Analogous equations were used for the other passbands.

Due to the long exposure times, the suitable airmass value for each frame was obtained by integrating the instantaneous airmass throughout the exposure. Following Stetson (1989) we approximated the integral by Simpson's rule with three points.

As indicated in Sect. 2, more than one standard star is usually present in the same field, giving a high weight to the airmass value when determining the extinction coefficients. To avoid this, we selected one/two standard stars per field, maintaining a wide range of colour indices, and the extinction coefficients were determined. With those fixed, the transformation to the standard system was completed in a second step, which then used all the standard stars present in the fields. The equations, based on Rosselló et al. (1985, 1988), are as follows:

$$\begin{aligned}
v - V &= a_1 + k_{V,BV}X_V + a_2(B-V) \\
&+ k'_{V,BV}X_V(B-V) + a_3(B-V)^2 \\
b - v &= b_1 + k_{B,BV}X_B - k_{V,BV}X_V + b_2(B-V) \\
&+ (k'_{B,BV}X_B - k'_{V,BV}X_V)(B-V) + b_3(B-V)^2 \\
u - b &= c_1 + k_{U,UB}X_U - k_{B,UB}X_B + c_2(U-B) \\
&+ (k'_{U,UB}X_U - k'_{B,UB}X_B)(U-B) + c_3(B-V) \\
v - r &= d_1 + k_{V,VR}X_V - k_{R,VR}X_R + d_2(V-R) \\
&+ (k'_{V,VR}X_V - k'_{R,VR}X_R)(V-R) + d_3(V-R)^2 \\
v - i &= e_1 + k_{V,VI}X_V - k_{I,VI}X_I + e_2(V-I) \\
&+ (k'_{V,VI}X_V - k'_{I,VI}X_I)(V-I) + e_3(V-I)^2 \\
v - V &= f_1 + k_{V,VR}X_V + f_2(V-R) \\
&+ k'_{V,VR}X_V(V-R) + f_3(V-R)^2
\end{aligned} \tag{3}$$

where a_i, b_i, c_i, d_i, e_i, f_i are the transformation coefficients.

The sixth equation was included to obtain V magnitude for those stars not detected with the B filter. For the stars detected with B, V and R filters, two V magnitudes were derived and they were averaged after checking their agreement.

The rms residuals of the standard stars in each observing night are shown in Table 4.

3.5. *Astrometry*

The Guide Star Catalogue Version 1 (GSC, Jenkner et al. 1989) was searched for the coordinates of the stars present in our fields. Unfortunately, the limiting magnitude of the GSC in the region of Cepheus OB3 is about $V = 14$ mag, so few stars in common were found. In the fields with four GSC stars (fields of BHJ 20 and 70), we took one of the stars as origin and we performed a least squares fitting of the equations

$$\begin{aligned}
\Delta\alpha\cos\delta &= a_0 + a_1\Delta x + a_2\Delta y \\
\Delta\delta &= b_0 + b_1\Delta x + b_2\Delta y
\end{aligned} \tag{4}$$

where Δ means the difference in the sense *star–origin*. The coefficients resulting from these fittings show a good alignment of $+y$ coordinate with $+\alpha$ and of $-x$ with $+\delta$. The coefficients a_1 and b_2 had very small absolute value (0.005″/pixel in average), showing that any possible rotation effect, if present, is not significant. So, $a_1 = b_2 = 0$ were adopted for the fields with three GSC stars (fields of BHJ 23, 27, 34 and 44). For the fields with less than three GSC stars, we also fixed the values of a_2 and b_1 to the average of the previous adjustments, and we applied this transformation taking as origin the available stars (one or two) and averaging the results.

No GSC star appears in the fields of BHJ 15 and BHJ 65. The only positional references for stars in these fields are PPM 24029=BHJ 15br and BD +62 2158=BHJ 65.

The resulting positions for program stars are linked to the reference system of the catalogue from which reference stars for their fields were taken. The given α and δ are for 2000.0 equinox. Although we give the positions in the field of BHJ 65 with a precision of 1″, one should bear in mind that they are relative to a BD position and so, their absolute accuracy is no better than 1′.

4. Results

The full process allowed us to derive photometry in the standard system for 1056 stars, with visual magnitude ranging from 8 to 21. The photometric data are given in Table 5 (only in electronic form). Individual errors were assigned to each star (each magnitude and each colour) as described below. An identification number was assigned to each star by taking the BHJ number of one of the stars present in the field and adding a second number by increasing right ascension. The cross identification with BHJ and other catalogues is given in notes. Stars centres are given as frame coordinates (x, y) and equatorial coordinates (α, δ) computed as described above.

Colour-magnitude and colour-colour diagrams are shown in Figs. 3, 4 and 5. Different symbols were used to plot members according BHJ, non-members according the same authors and stars not observed by them.

4.1. *Errors*

4.1.1. Internal errors

The internal errors of the standard magnitudes were evaluated from two different contributions: the errors in the instrumental magnitudes and the errors due

Table 4. Number of standard stars (N) and their rms residuals (σ)

Night	V_{B-V}		$B-V$		$U-B$		$V-R$		$V-I$		V_{V-R}	
	N	σ	N	σ	N	σ	N	σ	N	σ	N	σ
1991-11-05	22	0.021	21	0.018	22	0.027	23	0.014	23	0.023	22	0.021
1991-11-06	21	0.019	21	0.012	20	0.035	21	0.015	13	0.020	21	0.019
1991-11-07	20	0.026	20	0.018	17	0.018	20	0.015	20	0.020	20	0.026
1991-11-08	17	0.014	15	0.009	17	0.022	13	0.011	18	0.018	16	0.010
1991-11-09	21	0.014	20	0.010	19	0.030	21	0.012	20	0.023	21	0.014
1993-10-07	19	0.017	18	0.025	16	0.043	19	0.014	19	0.022	19	0.017

Table 6. Number of stars observed (N) and mean internal errors (σ) as a function of visual apparent magnitude

V range	V		$B-V$		$U-B$		$V-R$		$V-I$	
	N	σ	N	σ	N	σ	N	σ	N	σ
08-09	3	0.017	3	0.019	3	0.032	3	0.013	3	0.021
09-10	9	0.021	9	0.016	9	0.027	9	0.016	8	0.021
10-11	6	0.021	6	0.017	6	0.029	6	0.017	6	0.025
11-12	7	0.020	7	0.019	7	0.032	7	0.015	7	0.022
12-13	10	0.024	10	0.033	10	0.046	10	0.032	10	0.031
13-14	12	0.023	12	0.028	12	0.043	12	0.021	12	0.026
14-15	25	0.024	25	0.030	23	0.044	25	0.021	25	0.025
15-16	39	0.024	38	0.042	26	0.073	39	0.025	39	0.026
16-17	74	0.026	72	0.051	24	0.106	74	0.028	74	0.029
17-18	131	0.033	109	0.082	10	0.132	129	0.038	130	0.036
18-19	281	0.046	125	0.125			279	0.058	281	0.051
19-20	329	0.073	18	0.209			329	0.087	329	0.072
20-21	130	0.117					130	0.122	130	0.099
TOTAL:	1056		434		130		1052		1054	

to the transformation Eqs. (3). The errors in the instrumental magnitudes are given by PHOT and DAOGROW (Stetson 1987, 1990) as a function of photon-counting and the goodness of the fit of the growth curve. The rms residuals of the standard stars (Table 4) give the mean contribution of the transformation equations to the final errors. Both contributions were taken into account to compute the final errors adopted for our problem stars. So, the error of $B-V$ colour is

$$\Delta(B-V) = \sqrt{\frac{\Delta b^2 + \Delta v^2}{(b_2 + k'_{B,BV}X_B - k'_{V,BV}X_V)^2 - 4b_3[b_1 + k_{B,BV}X_B - k_{V,BV}X_V - (b-v)]} + \sigma^2_{BV}} \quad (5)$$

where σ_{BV} is the rms residual in $B-V$ of the standard stars, and Δb and Δv are the errors in the instrumental magnitudes b and v, respectively. Equivalent equations have been derived for $\Delta(V-R)$ and $\Delta(V-I)$.
The error for $U-B$ colour is given by:

$$\Delta(U-B) = \sqrt{\frac{\Delta u^2 + \Delta b^2 + {c_3}^2\Delta(B-V)^2}{(c_2 + k'_{U,UB}X_U - k'_{B,UB}X_B)^2} + \sigma^2_{UB}} \quad (6)$$

and for V magnitude when obtained with $B-V$ colour as:

$$\Delta V = \sqrt{\Delta v^2 + [a_2 + k'_{V,BV}X_V + 2a_3(B-V)]^2\Delta(B-V)^2 + \sigma^2_V} \quad (7)$$

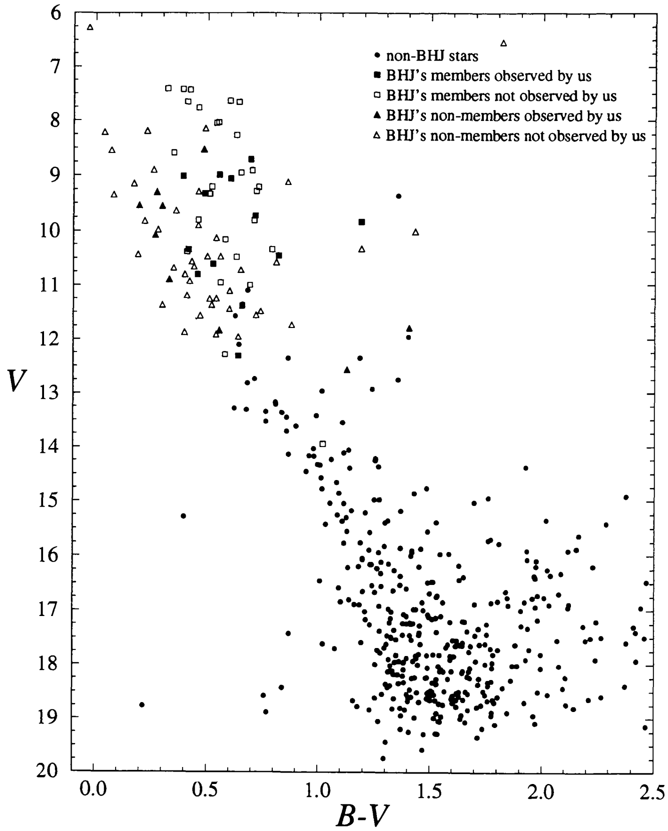

Fig. 3. Colour-magnitude diagram of the stars detected in the 18 fields of Cepheus OB3. Different symbols have been used for BHJ stars and the stars not observed by them

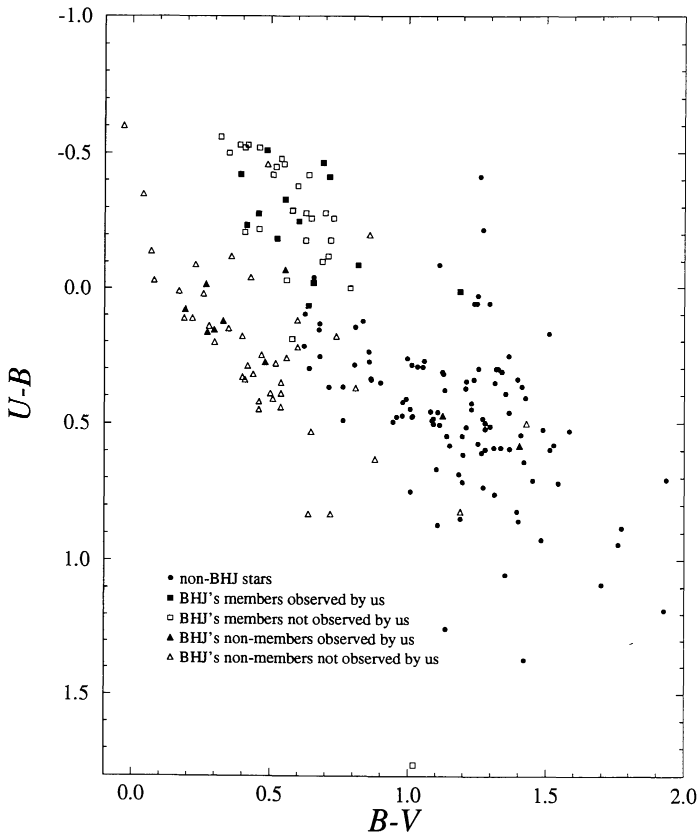

Fig. 4. Colour-colour diagram of the stars detected in the 18 fields of Cepheus OB3. Different symbols have been used for BHJ stars and the stars not observed by them

(an equivalent expression can be written for V magnitude obtained with $V-R$ colour).

The error for the bright stars is basically the contribution of the transformation equations (their instrumental errors are lower than or similar to those of the standard stars). In contrast, the error of the instrumental magnitudes is the main contribution to the final error for faint stars.

As described in Sect. 2, when the brightest star in the field became saturated due to the long exposure time, a shorter exposure was also taken. In this way, several stars of intermediate magnitude were recorded in both the short and long exposures. In this case, a mean weighted by the errors (Rosselló et al. 1985) was performed to derive the magnitude and colours from the two exposures.

Final errors as a function of visual magnitude are shown in Table 6 and Fig. 6.

4.1.2. External errors

Although Särg & Wrandemark (1970) have published *UBV* photometry in Cepheus region, there are only 4 stars in common with our observations and a significant comparison is not possible. Furthermore, there is not previously published *RI* photometry in this region. Every observed field contains at least one star observed by BHJ, and in total there are 22 stars in common. Doing the comparison, the stars showing significant departures from the main behaviour were omitted from the calculations: BHJ 15ft in V; BHJ 15ft, 17ft, 33ft, 44ft in $B-V$, and BHJ 15ft, 27 in $U-B$. The photometry for the ft stars could be uncertain due to the influence of the brighter companions. However, BHJ 27, which presents a difference of 0.45 mag in $U-B$, is a bright, isolated star with V and $B-V$ values fully compatible with BHJ's. So, the cause of the discrepancy is different and needs further analysis. Table 7 shows the average differences between our photometry and the values given by BHJ. The biggest average difference and dispersion are found for the $U-B$ index, due to the difficulty of CCD measurements at short wavelengths and to the well-known homogeinity problems with this index (Bessel 1990).

4.2. *Limiting magnitude of the sample*

Table 6 summarizes our CCD photometry as a function of apparent visual magnitude. For each V interval we give:

- N: total number of detected stars, and
- σ: average internal error for these stars.

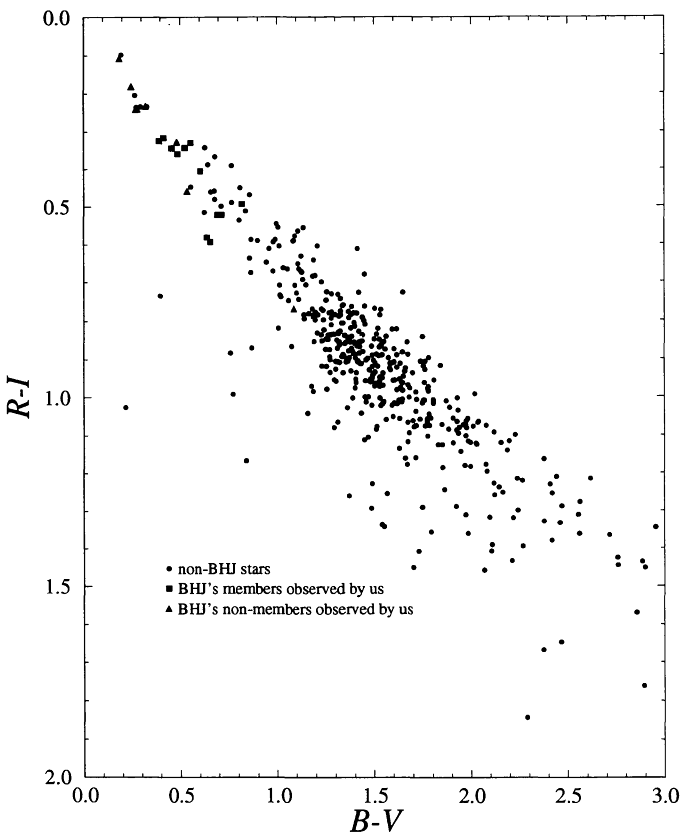

Fig. 5. Colour-colour diagram of the stars detected in the 18 fields of Cepheus OB3. Different symbols have been used for BHJ stars and the stars not observed by them

Table 7. External errors: BHJ - ours

	Mean (mag)	σ (mag)	No. of stars
ΔV	0.028	0.024	21
$\Delta(B-V)$	-.004	0.012	18
$\Delta(U-B)$	0.070	0.065	20

To determine the completeness limit of our sample, we performed automatic injection and recovery tests of artificial stars with DAOPHOT. We chose a set of six V frames, representative of the star density variety found in the selected fields. For each frame, the stellar PSF was determined and used to remove the stars detected. In addition, for each frame, a number of artificial stars equal to the number of stars detected was generated and injected. The instrumental magnitudes of these stars were decided randomly, following an exponential distribution fitted to the first magnitude intervals of Table 6, for which the sample completeness is reliable. The resulting frames were processed as the original ones. The comparison of the injected and recovered star lists allows us to evaluate the efficiency of the star-detection process. The test was performed more than a hundred times for each frame, to avoid small number statistics. The instrumental magnitudes of the artificial stars were transformed to the standard system. The conclusion is that the star detection is 100% efficient down to V=19 mag and the efficiency falls to negligible levels in an interval of one magnitude.

Although the star sample is 100% complete in V down to V=19 mag, we have completeness in all colour indices only down to V=15.5 mag. Visual magnitude and four colour indices have been determined for a total number of 130 stars.

Acknowledgements. P. Stetson of DAO has not only provided us his codes but he has also been permanently ready to solve problems and doubts with a diligence and humour worthy of gratitude. We wish to thank the staff of CAHA for their support during the observational runs and especially U. Thiele for his technical overview. We are grateful to J. Knude for his valuable comments. C.J. thanks A. Aguirre of CAHA for introducing her on the use of the MIDAS package. This work was supported by the DGICYT under contract PB91-0857 and *Ayudas para la utilización de recursos científicos de caracter específico* and CICYT under contract ESP94-1311-E. D.G.-E. also acknowledges the grant of the *Programa Sectorial de Formación de Profesorado Universitario y Personal Investigador* by the Ministerio de Eduación y Ciencia (ref. AP92 30526274).

References

Bessel M.S., 1990, PASP 102, 1181
Bessel M.S., 1993, Stellar Photometry –Current Techniques and Future Developements. Cambridge University Press, Cambridge, p. 22
Blaauw A., 1964, ARA&A 2, 213
Blaauw A., 1991, The Physics of Star Formation and Early Stellar Evolution. Kluwer Academic Publishers, Dordrecht, p. 125
Blaauw A., Hiltner W.A., Johnson H.L., 1959, ApJ 130, 69. (BHJ)
Brown A.G.A., De Geus E.J., De Zeeuw P.T., 1994, A&A 289, 101
Crawford D.L., Barnes J.V., 1970, AJ 75, 952
Da Costa G.S., 1992, Astronomical CCD Observing and Reduction Techniques. ASP Conf. Ser. 23, San Francisco, p. 90
De Geus D.J., De Zeeuw P.T., Lub J., 1989, A&A 216, 44
Galadí-Enríquez D., Jordi C., Trullols E., 1994, Proc. IAU Symp. 167 (in press)
Garmany C.D., 1992, A&AS 94, 211
Garmany C.D., 1994, PASP 106, 25
Garrison R.F., 1967, ApJ 147, 1003
Howell S.B., 1989, PASP 101, 616
Huges V.A., 1988, ApJ 333, 788
Jenkner H., Lasker B., McLean B., et al., 1989, The Guide Star Catalog. Space Telescope Science Institute, Baltimore
Jordi C., Trullols E., Rosselló G., Lahulla F., 1992, A&AS 94, 519
King I.R., 1971, PASP 83, 199
Landolt A.U., 1983, AJ 88, 439
Landolt A.U., 1992, AJ 104, 340

Rosselló G., Calafat R., Figueras F., et al., 1985, A&AS 59, 399

Rosselló G., Figueras F., Jordi C., et al., 1988, A&AS 75, 21

Särg K., Wrandemark S., 1970, A&AS 2, 251

Sargent A.I., 1979, ApJ 233, 163

Stetson P.B., 1987, PASP 99, 191

Stetson P.B., 1989, Highlights Astron. 8, p. 635

Stetson P.B., 1990, PASP 102, 932

Stetson P.B., 1993, Proc. IAU Coll. 136. Cambridge University Press, Cambridge, p. 291

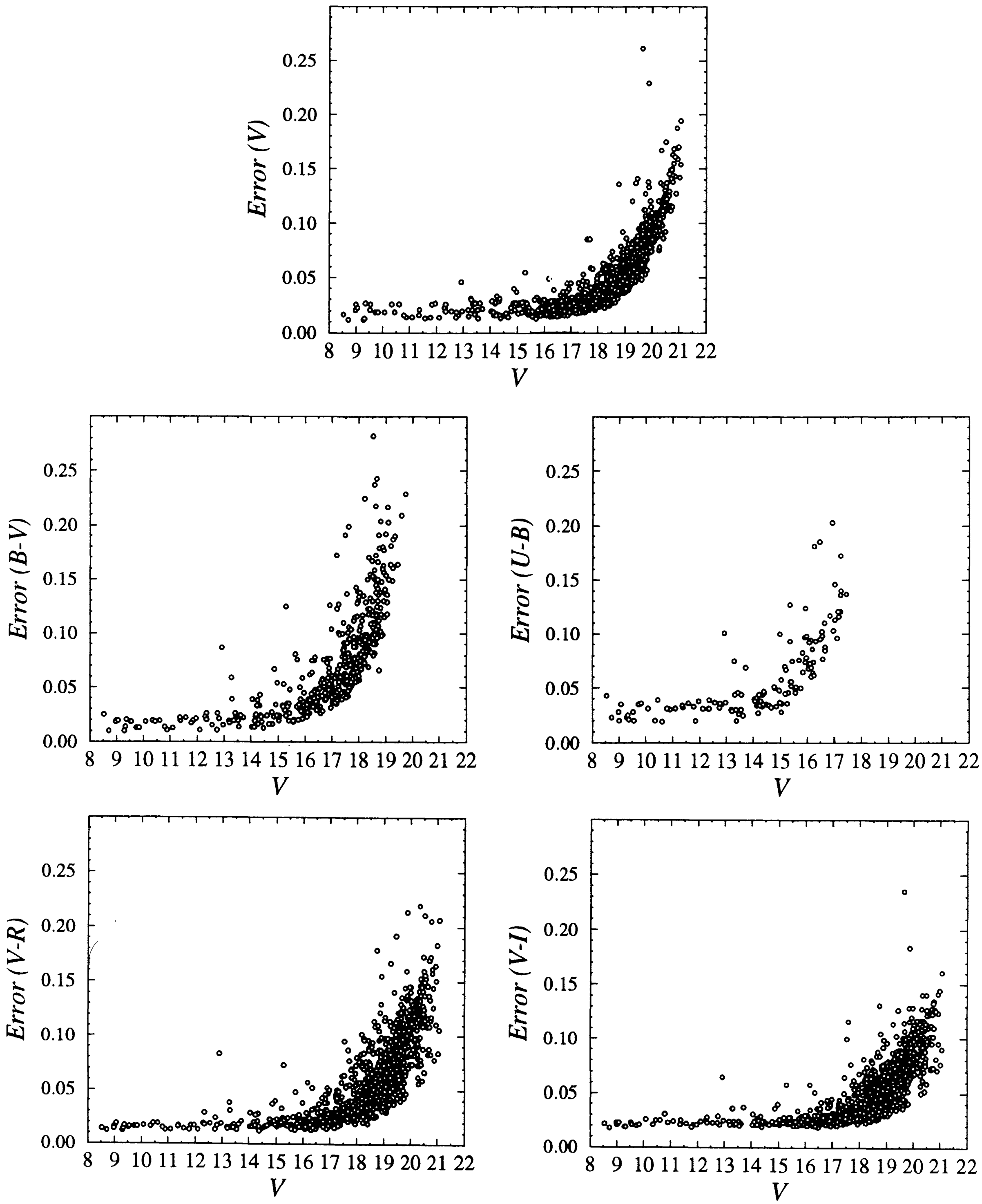

Fig. 6. Internal errors as a function of visual magnitude